Key Points:

- The 18-year trends of global-mean, clear-sky radiances at all Atmospheric Infrared Sounder (AIRS) thermal-infrared channels are analyzed
- AIRS observation shows statistically significant negative trends in most of its CO_2 channels and positive trends in some of its H_2O channels
- The best agreements between observations and reanalysis are seen over the CO_2 tropospheric channels

Correspondence to:
X. Huang,
xianglei@umich.edu

A Synopsis of AIRS Global-Mean Clear-Sky Radiance Trends From 2003 to 2020

Xianglei Huang[1] [ID], Xiuhong Chen[1] [ID], Chongxing Fan[1] [ID], Seiji Kato[2] [ID], Norman Loeb[2] [ID], Michael Bosilovich[3] [ID], Seung-Hee Ham[4] [ID], Fred G. Rose[4] [ID], and Lawrence L. Strow[5]

[1]Department of Climate and Space Sciences and Engineering, University of Michigan at Ann Arbor, Ann Arbor, MI, USA, [2]NASA Langley Research Center, Hampton, VA, USA, [3]NASA Goddard Space Flight Center, Greenbelt, MD, USA, [4]Science Systems and Applications, Inc., Hampton, VA, USA, [5]Department of Physics, University of Maryland at Baltimore County, Baltimore, MD, USA

Abstract Atmospheric Infrared Sounder (AIRS) aboard the National Aeronautics and Space Administration (NASA) Aqua satellite has been operating since September 2002. Its information content, superb instrument performance, and dense sampling pattern make the AIRS radiances an invaluable data set for climate studies. The trends of global-mean, nadir-view, clear-sky AIRS radiances from 2003 to 2020 are studied here, together with the counterparts of synthetic radiances based on two reanalyzes, European Centre for Medium-Range Weather Forecasts Reanalysis V5 (ECMWF ERA5) and NASA Goddard Earth Observing System V5.4.1 (GEOS-5.4.1; a reanalysis product without assimilation of hyperspectral radiances such as AIRS). The AIRS observation shows statistically significant negative trends in most of its CO_2 channels, positive but non-significant trends in the channels over the window regions, and statistically significant positive trends in some of its H_2O channels. The best agreements between observed and simulated radiance trends are seen over the CO_2 tropospheric channels, while the observed and simulated trends over the CO_2 stratospheric channels are opposite. ERA5 results largely agree with the AIRS observation over the H_2O channels. The comparison in the H_2O channels helps reveal a data continuity issue in the GEOS-5.4.1. Contributions from individual variables to the radiance trends are also assessed by performing separate simulations. This study provides the first synopsis of the global-mean trend of AIRS radiances over all its thermal-IR channels.

Plain Language Summary Using 18 years of satellite hyperspectral observations, we depict, for the first time, a synopsis of the trend of global-mean, clear-sky infrared radiances from ∼6 to ∼16 μm. Statistically significant trends are seen in the carbon dioxide and water vapor absorption bands but not over the infrared window region. The physical explanations of such trends are discussed and supported with simulation sensitivity studies. Such observed trends, channel-by-channel, are also compared with those derived from synthetic radiances based on reanalysis data sets. Discrepancies between observed and reanalysis-based trends are also discussed.

1. Introduction

The value of infrared (IR) hyperspectral radiance observations in climate sciences has been long recognized (e.g., Goody et al., 1998; Hanel & Conrath, 1970; Haskins et al., 1997; Iacono & Clough, 1996). Owing to the nature of IR radiative transfer, such observations contain plenty of information about temperature, humidity, and trace gas profiles, as well as clouds and dust aerosols. Besides providing global sounding profiles for numerical weather forecasts and monitoring trace gases that have absorption features in the infrared, IR hyperspectral radiance can play an important role in climate monitoring due to the excellent instrument performance and the dense sampling patterns of such observations. For example, Atmospheric Infrared Sounder (AIRS) aboard the National Aeronautics and Space Administration (NASA) Aqua satellite has a noise equivalent differential temperature of 0.2 K or even less for all its mid-IR channels (Aumann et al., 2006; Pagano et al., 2003) and its stability has been shown to be ∼2 mK/year (Aumann & Pagano, 2008). Since September 2002, AIRS has been collecting ∼3 million spectra every day with a global coverage within 2 days, except for several short periods due to instrument performance issues or satellite safety measures in response to solar flare storm. So far, AIRS has accumulated ∼22 billion well-calibrated spectra. Other IR hyperspectral sounders launched after AIRS, such as infrared atmospheric sounding interferometer (IASI) on Met-Op series of satellites and Cross-track Infrared Sounder (CrIS) on Suomi National Polar-orbiting Partnership and Joint Polar Satellite System series of satellites, have shown similar or

even better instrument performance than AIRS (Zavyalov et al., 2012). Therefore, by the end of this decade, we can expect to have three decades of well-calibrated record of IR radiances from space. Such a long data record will be invaluable to climate studies.

While such well-calibrated, stable-over-the-decade observations can be an ideal benchmark data set for climate studies, how to make full use of such observations is not trivial. Retrieval of IR spectral radiance observation, in the absence of any scattering process, is fundamentally an optimization of Fredholm integral equations of the first kind (Liou, 2002). Such optimization is known to be ill-posed, unstable, and could have unrealistic solutions. The mathematical nature of such retrieval limits the accuracy that can be achieved for each retrieval. Unlike passive microwave remote sensing, IR radiance is extremely sensitive to the presence of clouds, which makes the retrieval of all-sky observations even more challenging. Because of these limitations, it is attractive to keep a long-term record of radiances, spatially and temporally averaged, and use such radiance time series in climate studies. However, an inevitable fact then is how to physically interpret such radiance time series, that is, unscrambling "physical signals" from such time series for climate studies. It usually is also referred to as the "average-then-retrieve" approach. For example, Pan et al. (2017) applied the optimal fingerprinting technique to 10 years of AIRS radiances to estimate the stratospheric temperature and CO_2 trend in the presence of natural variability. Wu et al. (2020) used a principal component-based radiative transfer model (PCRTM; Liu et al., 2006) to develop a kernel-based technique to estimate anomalies of geophysical variables from spatially and temporally averaged radiance anomalies.

This study further explores the utility of such long-term spatially and temporally averaged radiances in climate studies, especially focusing on physical understanding and assessing the temperature and humidity information contained in such time series. Averages of all-sky radiances are challenging to interpret because clouds can vary significantly over spatial and temporal scales typically used in such an average (i.e., over a spatial grid of ∼100 km and a period of 1 month). Therefore, as a first endeavor, this study focuses on clear-sky radiances. We want to explore to what extent the available reanalysis and similar data products can reproduce the long-term characteristics in such observed radiance time series, and how such comparisons can be used to infer the issues in such long-term reanalysis products. Section 2 describes the data sets and data processing procedures, as well as the forward simulation to generate synthetic radiances from the reanalyzes. The assessments of the long-term trend, baseline difference, and the physical interpretation are then given in Section 3 and Section 4. Conclusions and reflections are then presented in Section 5. From frequency to frequency, the upwelling thermal-IR radiance intensity at the top of atmosphere can vary by more than a factor of 10. However, the brightness temperatures (BTs) at different frequencies vary only between 190 and 330 K over the entire globe. Therefore, depicting trends in BTs rather than radiance intensity is much easier for inter-channel comparisons. Because of this reason, the following sections will exclusively use BTs to discuss the trends over AIRS channels.

2. Data and Models

2.1. AIRS Radiances and Clear-Sky Footprint Selection

AIRS is a grating spectrometer aboard the NASA Aqua satellite and has collected data since September 2002 (Chahine et al., 2006). It measures three million spectra per day with a scanning angle up to ±49°. By the end of 2021, more than 22 billion spectra have been collected by AIRS. It has 2,378 channels with spectral coverage from 3.7 to 15.4 μm, with several spectral gaps in between. The shortwave IR channels are not used here due to the overlapped information content with the mid-IR channels and the additional complexity of considering solar radiation for daytime measurements at such channels. Thus, our analysis is limited to 1,864 channels between 6.2 and 15.4 μm (i.e., 649.6–1613.9 cm^{-1}). AIRS has a spectral resolving power ($\lambda/\delta\lambda$) of 1,200, that is, a varying spectral resolution from ∼0.5 cm^{-1} at the low end of the mid-IR frequency range to 1.34 cm^{-1} at the high end. The on-orbit radiometric calibration accuracy of AIRS measurement has been shown to be better than 0.2 K (Aumann et al., 2006). Its stability was initially estimated to be ∼4 mK yr^{-1} (Aumann & Pagano, 2008). Strow and DeSouza-Machado (2020) evaluated the stability of more than 400 AIRS channels and showed the stability of these channels is ∼2 mK yr^{-1}.

The spectral calibration of AIRS has also been shown to be stable and shift no more than 0.1% of a full-width half maximum. The BT trends caused by the shift of spectral response function (SRF) can be estimated using the method described in Strow et al. (2006) and Pan et al. (2017). Following the methodology described in Pan
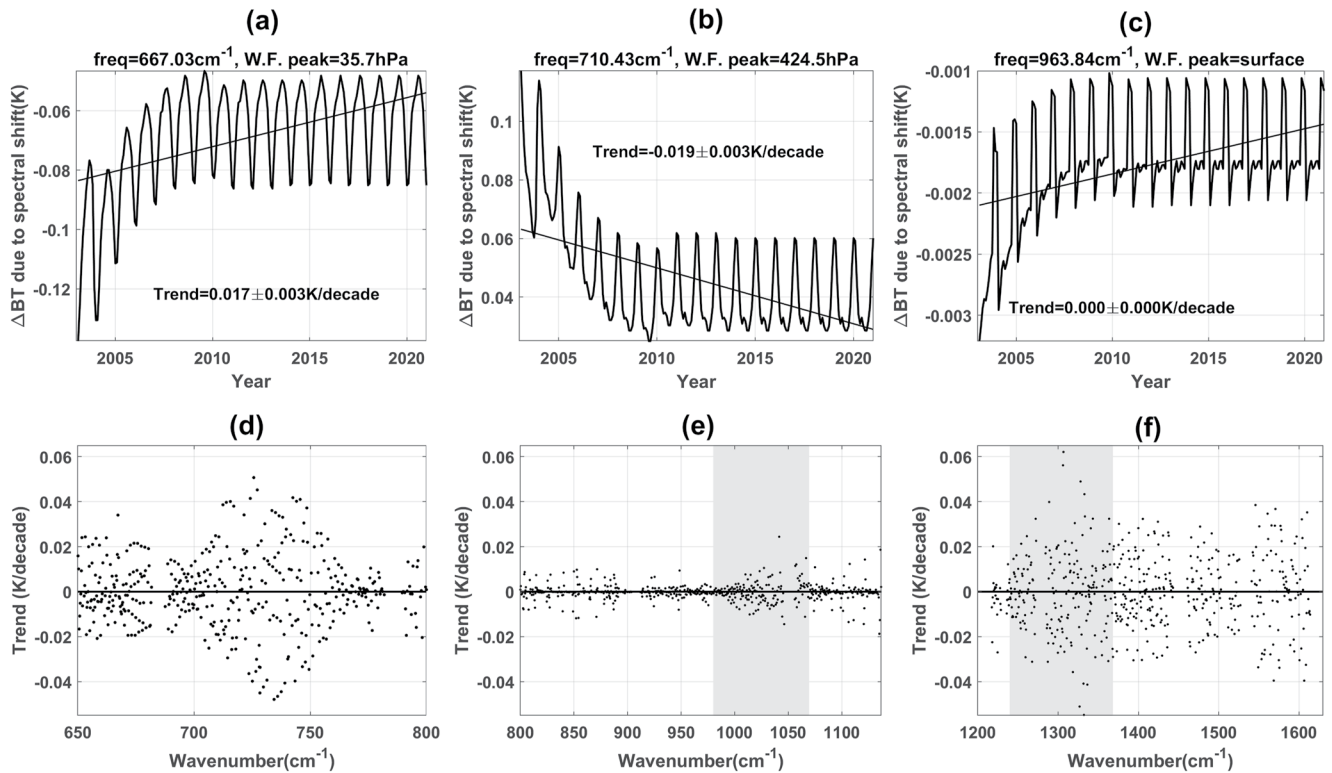
Figure 1. Upper panels: the change of brightness temperature (ΔBT) due to spectral shift with time at three Atmospheric Infrared Sounder (AIRS) channels, two in the CO_2 band and one in the window region. The peak of the clear-sky weighting function (W.F.; based on 1976 US standard atmosphere) for each channel is labeled on the title. Lower panels: the linear trend of ΔBT due to spectral shift for all the AIRS mid-IR channels. The trend is for 2003–2020. The gray shade columns indicate spectral regions with strong absorptions by trace gases other than H_2O and CO_2 (i.e., ozone for 980–1,070 cm^{-1} and N_2O and CH_4 for 1,240–1,368 cm^{-1}).

et al. (2017), we estimated the BT bias due to such shift of SRF for each AIRS channel and for each month, termed as ΔBT_shift(t, ν), and applied such spectral shift correction to the data month by month. Figure 1 shows the time series of ΔBT_shift for three AIRS channels, 667.03, 710.43, and 963.84 cm^{-1}, as well as the linear trend of such ΔBT_shift(t, ν) for all AIRS channels used in this study. The ΔBT caused by such spectral shift was ∼0.1 K or less in magnitude at the beginning of the operation and usually stabilized at a much smaller magnitude (with apparent seasonal cycle) after 2009. The overall trend caused by such spectral shift is within ±0.02 K/decade for all the channels, which is one order of magnitude smaller than the trends to be discussed in the following sections.

To avoid impact of different viewing zenith angles on radiance average, we only use AIRS spectra within ±5° scanning angle in this study. Given cos5° = 0.996, all observations used here can be deemed as nadir-view. Quality control procedures as in Huang and Yung (2005) are applied to each AIRS spectrum to exclude abnormal channels. To select clear-sky footprints, each individual AIRS footprint is collocated with the Aqua CERES (The Clouds and the Earth's Radiant Energy System) footprint, using procedures described in Huang et al. (2008). The CERES Single Satellite Footprint data product has a sophisticated algorithm for clear-sky detection (Minnis et al., 2020), using Moderate Resolution Imaging Spectroradiometer (MODIS) imageries within each CERES footprint. A CERES footprint with a cloud fraction less than 1% is deemed clear-sky (Loeb et al., 2003). Similar to Huang et al. (2008, 2014), all identified clear-sky AIRS spectra within a 16-day period are then further averaged onto regular 2.5° longitude by 2° latitude grids. Sixteen days is the orbital repeating cycle of the Aqua satellite, which makes a homogeneous sampling pattern for nadir-view observations. A monthly average is also tested and shows little difference from such 16-day average results as far as the trends of radiances are concerned.

2.2. GEOS-5.4.1 and ERA5 Reanalysis

We use two sets of reanalysis products, that is, GEOS-5.4.1 and ERA5 reanalyzes, to simulate AIRS clear-sky nadir-view radiances (hereafter, referred to as synthetic AIRS radiances), respectively. The GEOS 5.4.1

reanalysis system is largely based the system used to perform the NASA Modern-Era Retrospective analysis for Research and Applications (MERRA) reanalysis system (a.k.a. GEOS 5.2.0; Rienecker et al., 2008, 2011), with some specific requirements to support the CERES science team's need of producing climate data record products. An important difference from other commonly used reanalysis products is that the GEOS 5.4.1 intentionally does not assimilate the hyperspectral radiances (such as AIRS, CrIS, and IASI) and Global Position System occultation observations. Compared to the MERRA reanalysis, some model changes in the GEOS 5.4.1. include an update to the Relaxed Arakawa-Schubert convection parameterization to include resolution dependent stochastic limitation of cumulus entrainment and time-varying aerosols for radiation calculations. Some surface constants were updated to address a cold bias over snow, along with several other minor updates. Its 3-hourly temperature and humidity products have a horizontal resolution of 0.5° in latitude and 0.67° in longitude, with 42 pressure levels in vertical up to 0.1 hPa.

ERA5 reanalysis is the fifth-generation global atmospheric reanalysis produced by the European Centre for Medium-Range Weather Forecasts. It is based on Integrated Forecasting System Cycle 41r2 4D-var assimilation system with a 31-km horizontal resolution and 137 model vertical levels and output hourly analysis fields. It has been widely used by the climate community for a variety of analyses and comparisons. AIRS radiances have been assimilated into the ERA5 reanalysis using the method described in McNally et al. (2006). An algorithm to identify cloud-contaminated channels (McNally & Watts, 2003) has been used to select channels unaffected by clouds, and only such channels could be assimilated into the ERA5 reanalysis. More details about the ERA5 reanalysis can be found in Hersbach et al. (2020).

2.3. Simulation of AIRS Clear-Sky Radiances and Comparisons With Global-Mean Observations

To simulate the AIRS clear-sky radiances, 3-hourly (GEOS-5.4.1) or 6-hourly (ERA5) atmospheric temperature, humidity, and ozone profiles and surface temperature and pressure are fed into PCRTM (Liu et al., 2006) to generate synthetic AIRS radiance. PCRTM is a fast radiative transfer model utilizing the correlations among AIRS channels to simulate the full AIRS spectral radiances. Compared to benchmark line-by-line radiative transfer calculation, PCRTM has a satisfactory performance with a root-mean-square difference of 0.67 K in BT but 4,480 times faster (Chen et al., 2013), making it ideal for such a vast amount of hyperspectral radiance simulations. The biases in PCRTM simulation are also small and less relevant to the trend analysis examined here. Besides time-varying water vapor and ozone fields from the reanalysis, monthly global-mean CO_2 concentration compiled by National Oceanic and Atmospheric Administration Global Monitoring Laboratory using the surface observations (Dlugokencky & Tans, 2021) is also used in the simulation. The rest of the greenhouse gases, such as N_2O and CH_4, are kept unchanged since our focus here is on water vapor and temperature. Correspondingly, the AIRS channels significantly affected by N_2O and CH_4 absorptions (1240–1360 cm^{-1}) are excluded in our following trend studies. The surface spectral emissivity is based on a global monthly varying surface spectral emissivity data set compiled in Huang et al. (2016). For the spectral region covered by the AIRS mid-IR observations, the surface spectral emissivity in Huang et al. (2016) is largely based on the surface spectral emissivity retrieved from MODIS observation (Seemann et al., 2008).

After such 3-hourly (or 6-hourly) synthetic AIRS spectra over the entire globe have been generated, the radiances are further linearly interpolated, spatially and temporally, to the same time and location as the AIRS clear-sky observation described in Section 2.1. Then such interpolated radiances are processed in the same way as AIRS data to form gridded data for trend analysis. Figure 2 shows the simulated and observed global-mean AIRS radiance over the entire period of 2003–2020. As time-varying CH_4 is not considered in the simulation, differences between simulations and the AIRS observation over the center of CH_4 Q-branch (~1,306 cm^{-1}) can be more than 1 K in BT (Figure 2f). The differences over the O_3 band can be as large as ~0.7 K in BT (Figure 2e). For clear-sky radiances, the mid-IR ozone band is almost equally affected by surface emission and stratospheric ozone absorption and emission because, unlike the CO_2 16.7 μm band, the center of this ozone band is not opaque enough, and a considerable amount of the surface emission can still reach the top of the atmosphere. Such differences over the O_3 band are larger than the differences over the neighboring window region, suggesting the difference in the stratosphere (temperature or ozone or both) must play a role here. Even though the reanalysis ozone profiles have been used in our calculation, given the focus of this study being temperature and humidity, the radiances from AIRS channels in the ozone band will not be analyzed in the following sections, too, just like those in the N_2O and CH_4 bands.
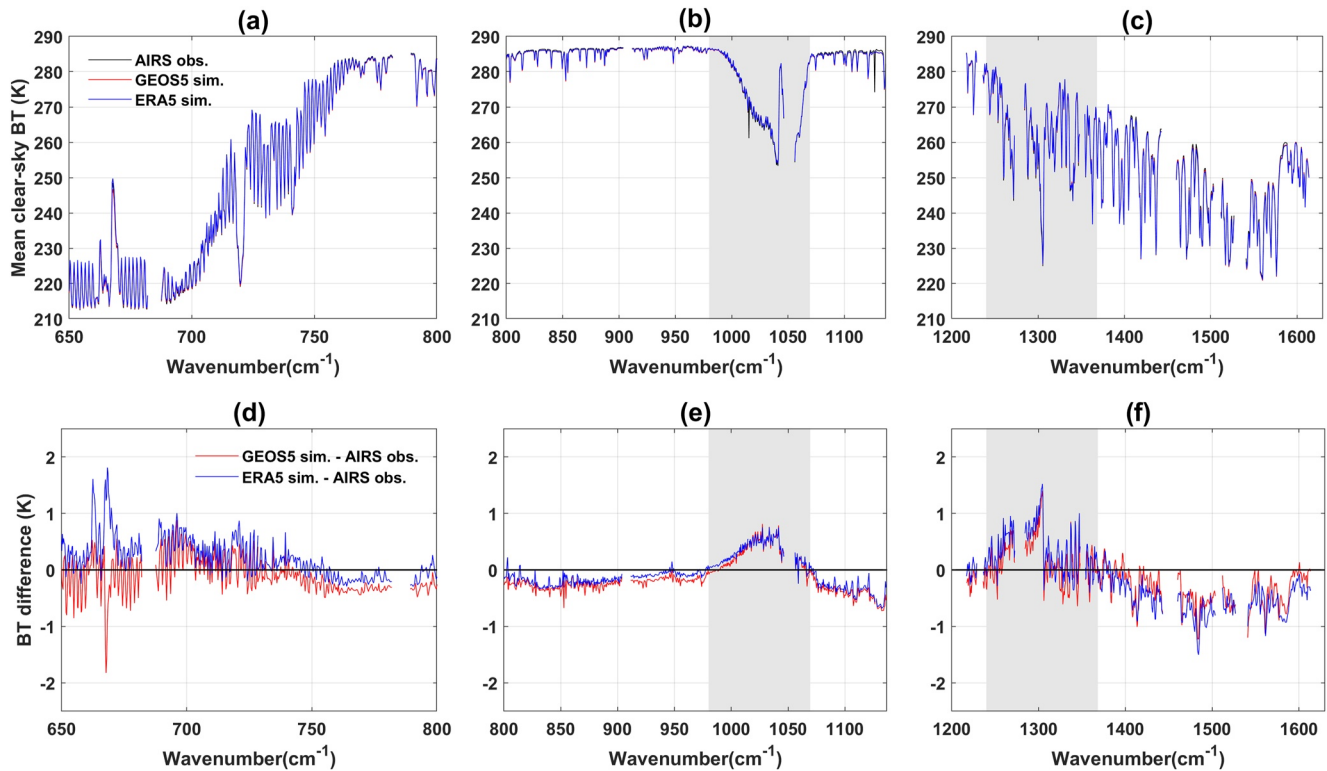
Figure 2. (a–c): The observed and simulated nadir-view, global-mean Atmospheric Infrared Sounder (AIRS) spectral radiances averaged from 2003 to 2020. The entire spectrum is broken into three panels for better visualization. (d–f): The difference between simulated and observed global-mean AIRS radiances shown in the (a–c), GEOS5 results are shown in red and ERA5 results in blue. Same as Figure 1, the gray shade columns indicate spectral regions with strong absorptions by trace gases other than H_2O and CO_2 (i.e., ozone for 980–1,070 cm^{-1} and N_2O and CH_4 for 1,240–1,368 cm^{-1}).

Besides the O_3, N_2O, and CH_4 bands, the simulation-observation difference is also noticeably large in the center of CO_2 bands (660–678 cm^{-1}), that is, channels sensitive to the stratospheric emissions and absorptions. Unlike the three bands mentioned above, two differences here, that is, GEOS5—AIRS, and ERA5—AIRS, have opposite signs. Given the same set of CO_2 values have been used in the simulation, this can only come from the differences in reanalysis stratospheric temperature: 18-year global mean stratospheric temperature in the ERA5 could be higher than its counterpart in reality and, in contrast, GEOS-5 could have a colder stratosphere than the reality. For the rest of the channels, that is, tropospheric channels in the CO_2 band, window channels, and all channels in the H_2O band except those overlapped with N_2O and CH_4 bands, the long-term mean differences between simulations and AIRS observations are usually within ± 0.5 K in BT.

3. Time Series and Trends of Four Representative AIRS Channels

This section examines the time series and the linear trends of radiances at four representative AIRS channels. As in Pan et al. (2015, 2017), all trends are obtained by linear regression, and associated uncertainties are estimated according to Weatherhead et al. (1998), which takes the autocorrelation time scale of the time series into account. As in Figures 1 and 2, all discussions will be in BT.

Four channels are (a) 667.03 cm^{-1}, a channel at the center of the CO_2 band sensitive to the mid-stratosphere; (b) 710.43 cm^{-1}, a channel also in the CO_2 band but sensitive to the mid-troposphere under the clear sky; (c) 963.84 cm^{-1}, one of the most transparent channels in the window region, with a transmissivity of 0.94 for the 1976 US standard atmosphere profile; (d) 1596.32 cm^{-1}, a channel at the center of H_2O v_2 band and sensitive to the mid-troposphere under the clear sky.
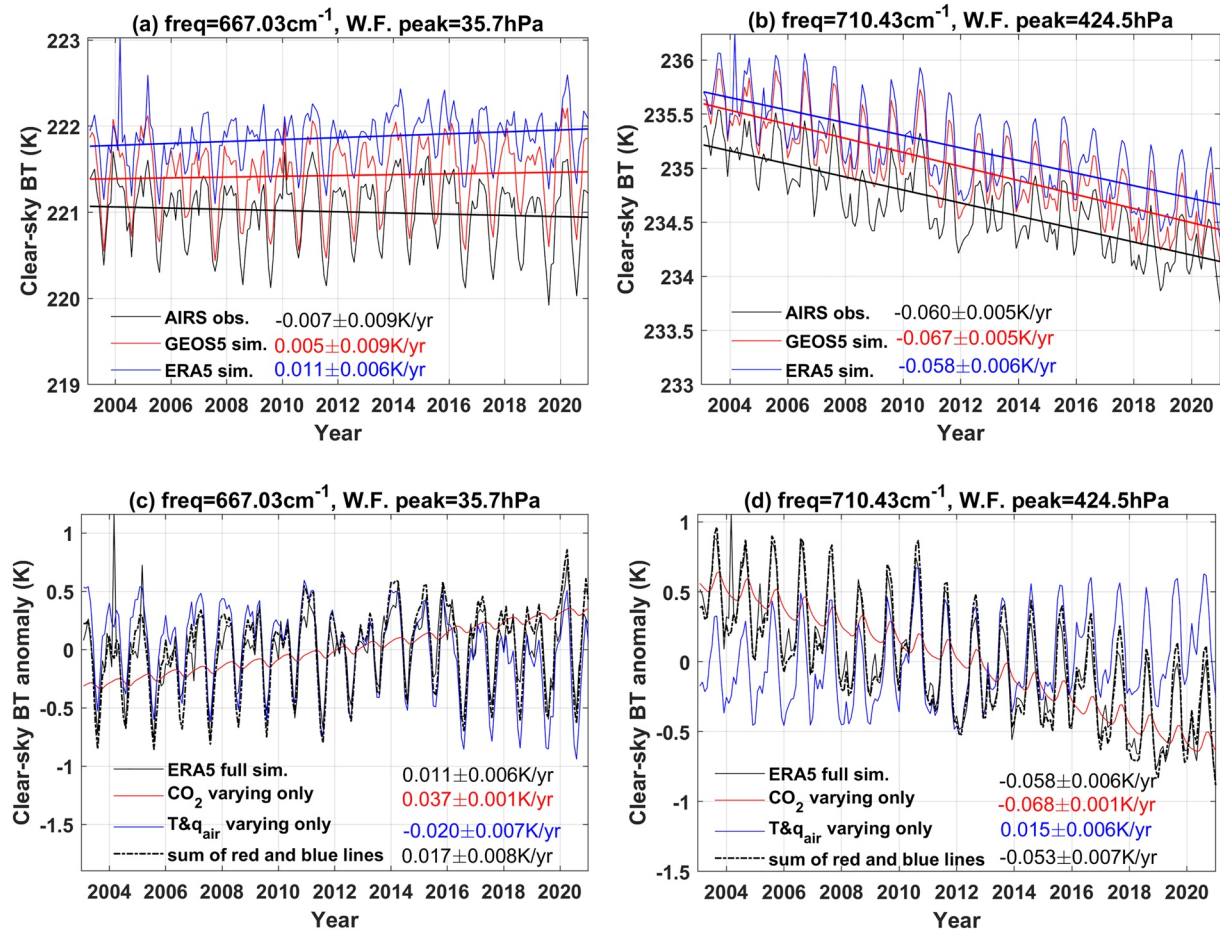
Figure 3. (a) The observed and simulated global-mean time series of Atmospheric Infrared Sounder (AIRS) nadir-view, clear-sky radiances at 667.03 cm^{-1}, a middle-stratospheric channel. The linear trends with 95% confidence intervals are also labeled on the plot. (b) Same as (a) but for the AIRS channel at 710.43 cm^{-1}, a middle-tropospheric channel. (c) The black line is the time series of simulated clear-sky brightness temperature anomaly based on ERA5 reanalysis, as shown in (a). The rest three lines are based on ERA5 monthly mean profiles: the red line is anomaly time series when only CO_2 varies with time, but temperature and humidity profiles are fixed at their respective values of January 2003; the blue line is radiance anomaly time series when CO_2 was fixed at its value in January 2003 but temperature, and humidity profiles change with time. The black dash-dotted line is the summation of the red and blue lines. All anomalies are deviations from their respective mean over the entire period. (d) Same as (c) except for the 710.43 cm^{-1} channel.

3.1. Two Channels in the CO_2 Band

The observed and simulated time series of the two CO_2 channels are shown in Figures 3a and 3b, respectively. ERA5 has a statistically significant positive trend, 0.11 ± 0.06 K/decade (95% confidence interval) at the 667.03 cm^{-1} channel, while the trends from AIRS observations and GEOS5 are not statistically significant (i.e., not significantly different from zero) Note the linear trend from AIRS observations is negative, while both ERA5 and GEOS5 have positive trends. In contrast, both reanalyzes and AIRS observation agree well on the trend at the 710.43 cm^{-1} channels, all showing a statistically significant negative trend around −0.63 ± 0.06 K/decade.

The trends in such CO_2 channels are determined by two components. First, as CO_2 increases, the optical depth (τ) will increase at all vertical levels. As a result, the peak of the weighting function, which is around the level where $\tau = 1$, will shift upward. If the temperature had remained constant at the same time, such CO_2 change alone would have led to a positive trend in BT for the stratospheric channel (because stratospheric temperature increases with altitude) and a negative trend in BT for the tropospheric channel (because tropospheric temperature decrease with the altitude). Second, the temperature also changes in response to the increase of CO_2. It is well known that the stratosphere becomes cooler as CO_2 increases to restore the radiative equilibrium (Manabe & Wetherald, 1967; Ramaswamy et al., 2006) and the troposphere becomes warmer due to the radiative feedbacks in response to surface warming resulting from the increase of CO_2 (Raghuraman et al., 2019; Ramaswamy et al., 2019). The
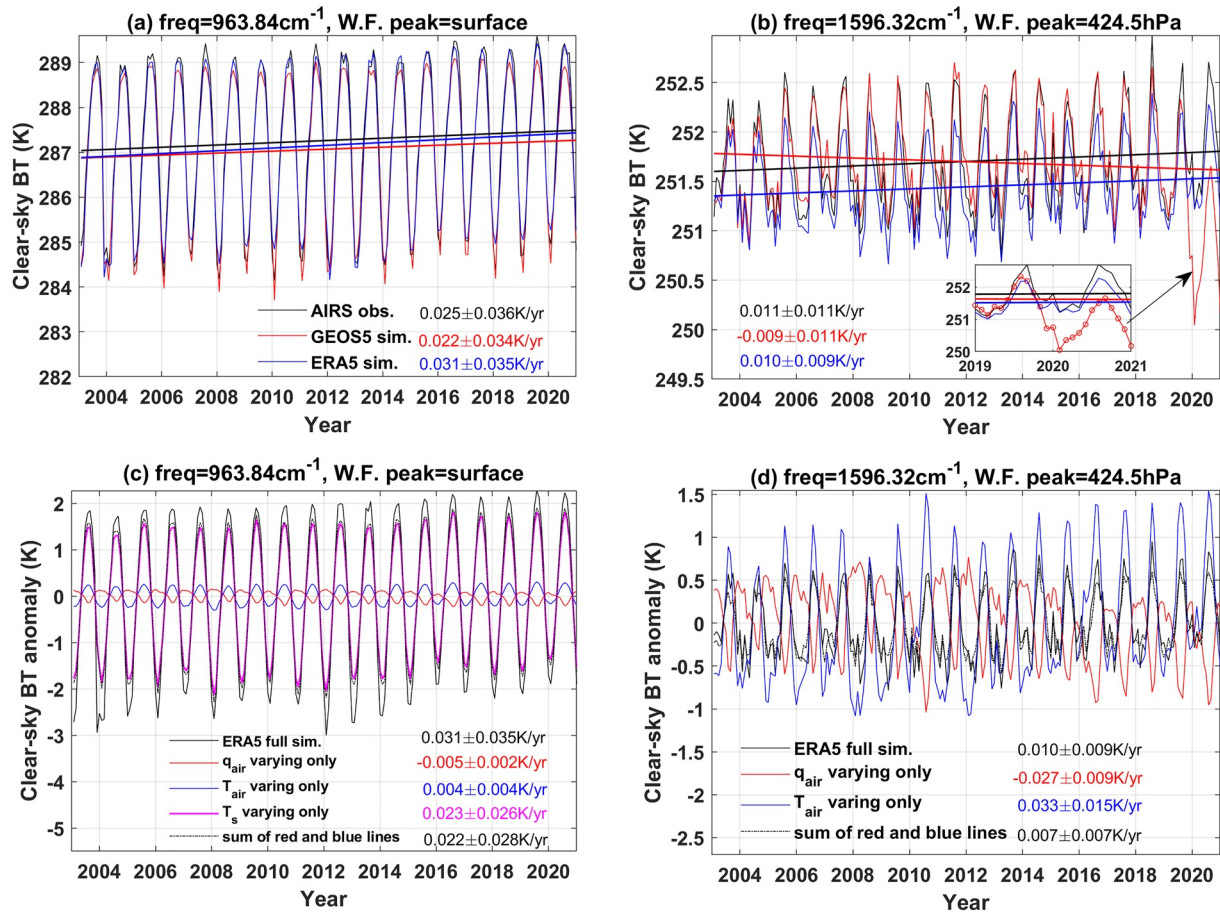
Figure 4. Similar to Figure 3 but for a mid-IR window channel at 963.84 cm^{-1} and an H$_2$O channel at 1596.32 cm^{-1}. In (c), the anomalies by varying surface temperature (T$_s$) only and by varying atmospheric temperature (T$_{air}$) are shown as pink and blue lines, respectively. In (d), the anomaly by varying T$_s$ is not shown as this channel has zero sensitivity to surface emission.

stratospheric changes are fast, usually within a few weeks, while the tropospheric changes in response to surface warming are much slower. Therefore, the actual temperature change alone would leave a negative trend in the stratospheric channels and a positive trend in the troposphere channels. Thus, the contributions of CO$_2$ and temperature long-term changes to the trend of BT are opposite to each other for both the stratospheric and tropospheric channels.

To quantify the contributions of such two components, we use ERA5 monthly mean profiles to carry out two additional sets of sensitivity simulations: one set uses the time-varying CO$_2$, but the temperature and humidity profiles and surface temperatures are fixed at the values for January 2003 (red lines in Figures 3c and 3d); the other set uses actual ERA5 profiles for each month but fixed CO$_2$ at the level of January 2003 (blue lines in Figures 3c and 3d). The summation of clear-sky BT anomalies computed from the two sensitivity simulations can match the anomalies from the full ERA5 very well (black dash lines in Figures 3c and 3d), as does the summation of the linear trends from the two sensitivity simulations with the trends from the full simulation. The linear trend due to CO$_2$ increases is 0.37 ± 0.01 K/decade for the 667.03 cm^{-1} channel and -0.68 ± 0.01 K/decade for the 710.43 cm^{-1} channel. The linear trends due to temperature change are smaller in amplitude than the linear trends caused by CO$_2$ but in opposite signs. As a result, for the ERA-5 synthetic AIRS radiances, the overall trend is positive for the stratospheric channel and negative for the tropospheric channel.

3.2. A Window Channel at 963.84 cm^{-1}

The observed and simulated times series at a window channel, 963.84 cm^{-1}, is shown in Figure 4a. Among all four individual channels examined in this section, this channel shows the smallest baseline differences
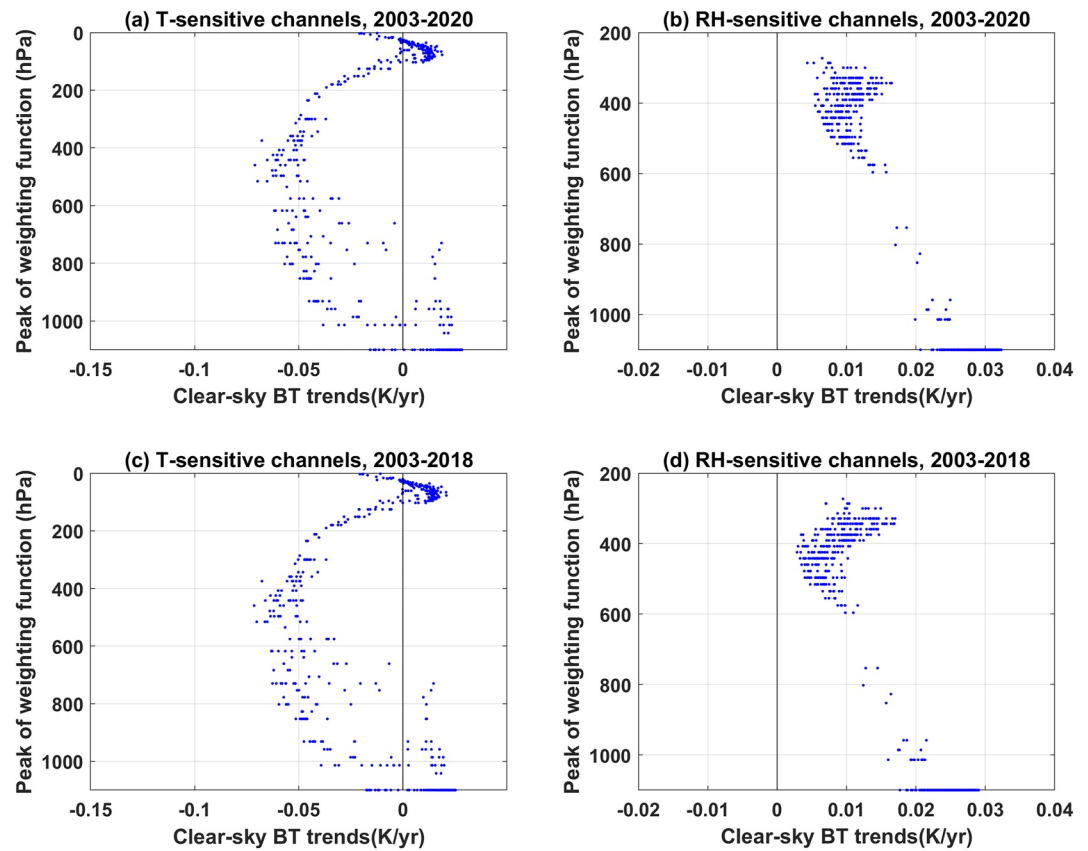
Figure 5. (a) Scatter plot of the linear trends of simulated global-mean, nadir-view Atmospheric Infrared Sounder clear-sky radiances over channels in the CO_2 band (terms as temperature-sensitive channels) with respect to the peaks of clear-sky weighting functions of corresponding channels. The trends are derived from the ERA5-based synthetic radiance over the 2003–2020 period. The weighting function is computed using the US 1976 standard atmosphere. (b) Same as (a) but for channels in the window region and H_2O bands (terms as relative-humidity-sensitive channels). (c) Same as (a) except for the 2003–2018 period. (d) Same as (b) except for the 2003–2018 period. Note for all the channels shown here, the 95% confidence interval of the trend derived from 2003 to 2020 period overlaps with their counterpart from the 2003–2018 period.

between observation and simulations. Such a good agreement is not a surprise since this channel is overwhelmingly influenced by surface temperature, a quantity well assimilated in both reanalyzes. All three time series show a positive but statistically insignificant trend around 0.22–0.31 K/decade. Using a similar approach as described in Section 3.1, we further use ERA5 reanalysis to assess the individual contributions to the trend.

As expected, the largest contribution comes from surface temperature (pink line in Figure 4c). When only atmospheric temperature or humidity profiles vary with time (blue and red lines in Figure 4c), they can contribute to the time series through the water vapor continuum absorption and emission at this channel, but their contributions have a much smaller seasonal cycle and are out of phase with each other. This can be understood in the following way: temperature and humidity variations in the boundary layers are in phase; however, an increase in atmospheric temperature alone leads to more atmospheric emission to the space, while an increase of water vapor alone has two competing effects: absorb more surface emission (so less surface emission reaches the space) and emit more atmospheric radiation. The net effect of water vapor increase in the planetary boundary layer (PBL) is a reduction of radiance reaching the space because the temperature in the PBL is generally lower than the surface temperature. Thus, the net effect of water vapor increase is out of phase with the effect of atmospheric temperature increase. As a result, the linear trend due to atmospheric temperature variation largely offsets the linear trend due to atmospheric humidity variation.
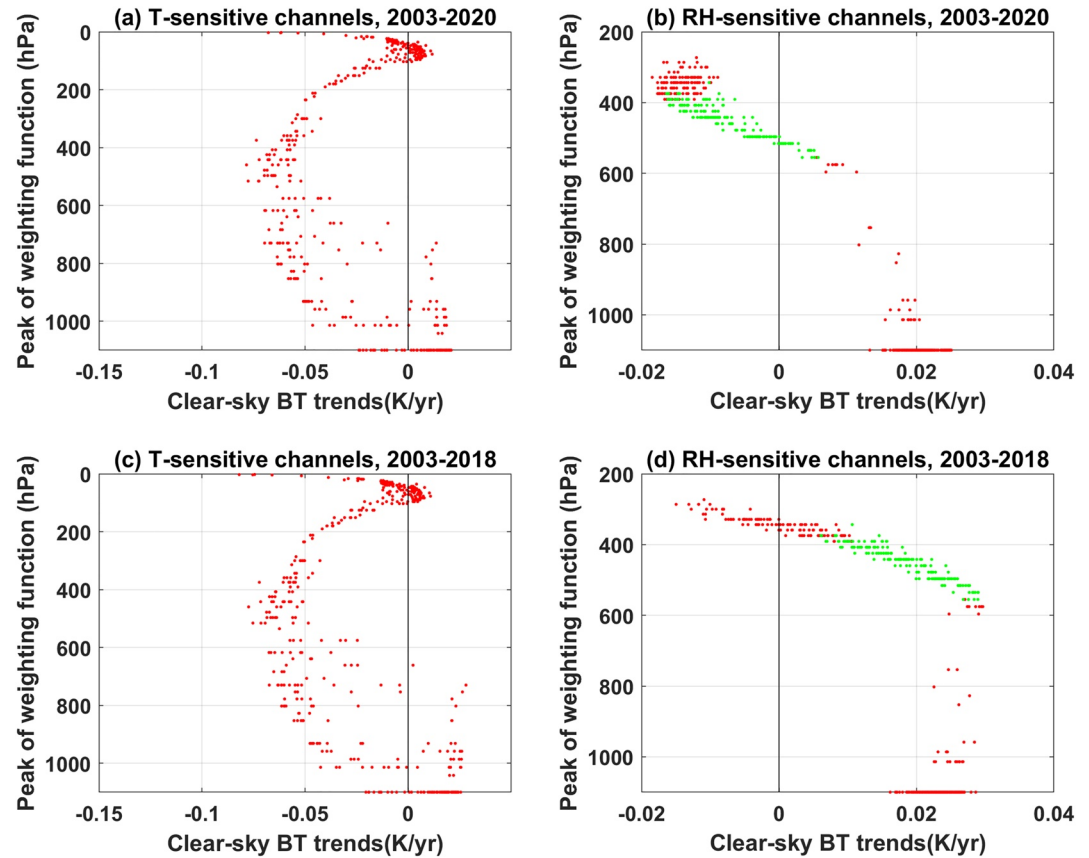
Figure 6. Same as Figure 5 but derived from synthetic Atmospheric Infrared Sounder radiances based on the GEOS-5.4.1 data. Green dots denote channels of which the 95% confidence interval of the trend derived from 2003 to 2020 period does not overlap with their counterpart from 2003 to 2018 period. Like the ERA5 case in Figure 5, trends over all T-sensitive channels change little between two periods. Trends over the RH-sensitive channels with peaks of weighting functions around 400–600 hPa show statistically different trends between the two periods, which is due to the issues in GEOS-5 assimilation discussed in the text.

3.3. The Water Vapor Channel at 1596.32 cm^{-1}

3.3.1. Impact of the MHS Failure in November 2019

Figure 4b shows the observed and simulated time series of clear-sky radiances at 1596.32 cm^{-1}, a channel at the center of the H_2O v_2 band, and sensitive to mid-tropospheric water vapor emissions and absorptions. The most noticeable difference among the three time-series is the sudden drop of the GESO-5 time series after November 2019. A careful examination of GEOS-5 data showed that the Microwave Humidity Sounder (MHS) on the European MetOp-A satellite, which was assimilated by GEOS-5, has had a channel failure since 15 November 2019 (ESPC Operations, 2020), and GEOS-5 data assimilation did not properly consider this failure. GEOS-5 data product since then was inadvertently affected by this MHS failure. To further confirm this cause and assess the impact of this on the synthetic AIRS radiance trends, we calculated the linear trends for two periods, 2003–2018 and 2003–2020, and for all relevant AIRS channels. For AIRS channels sensitive to the temperature but not to water vapor (i.e., channels in the CO_2 band, termed T-sensitive channels), the linear trends derived from the two periods are the same for both the ERA5 and GEOS-5 results (Figures 5a and 5c for ERA5, and Figures 6a and 6c for GEOS-5): the 95% confidence intervals of the trends derived from 2003 to 2020 period overlap with the counterparts derived from 2003 to 2018 period for all the channels. For AIRS channels sensitive to both temperature and humidity (i.e., channels in the window region and H_2O band, termed RH-sensitive channels, where RH stands for relative humidity), the linear trends derived from two periods are the same for the case of ERA5 synthetic radiance (Figures 5b and 5d); but are different for the case of GEOS-5 synthetic radiance (Figures 6b and 6d). Specifically, the GEOS-5 trends between the two periods differ the most for the channels that have peaks of their
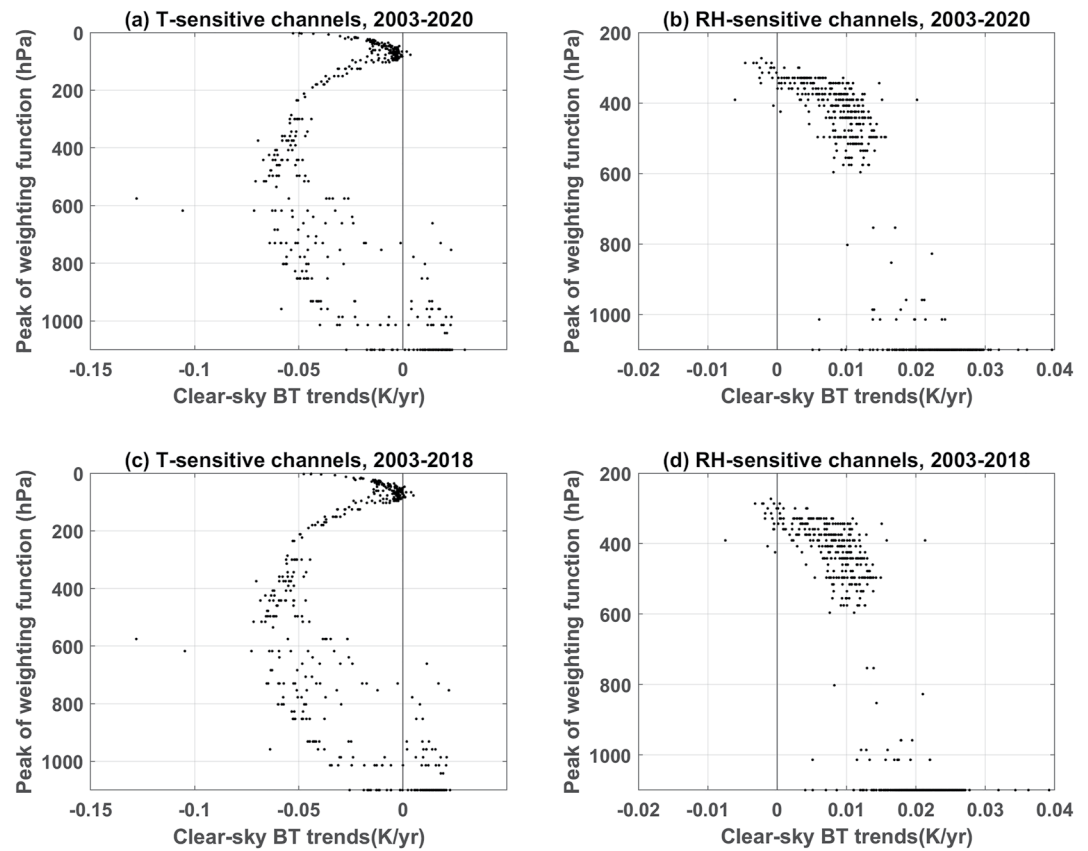
Figure 7. Same as Figure 5 but based on actual Atmospheric Infrared Sounder observations. Note for all the channels shown here, the 95% confidence interval of the trend derived from the 2003–2020 period overlaps with their counterpart from the 2003–2018 period. Just like the case of ERA5 in Figure 5, all the trends derived from two periods, that is, 2003–2020 versus from 2003 to 2018, are largely similar to each other.

clear-sky weighting functions around 300–700 hPa. Note that the green dots in Figures 6b and 6d denote channels where the 95% confidence intervals of the trends derived from the two periods do not overlap. For example, the trends for the channels with a peak of their clear-sky weighting function around 350–500 hPa are positive for the 2003–2018 period (Figure 6d) but negative for the 2003–2020 period (Figure 6b), which is due to the artificial drop of the radiance after November 2019 (like what has been shown in Figure 4b). For comparison, the trends from AIRS observations are plotted in the same way in Figure 7. Consistent with the case of ERA5, AIRS trends derived from 2003 to 2018 are largely the same as those derived from 2003 to 2020, the 95% confidence intervals of the trends derived from the two period always overlap for all the channels. This further confirms that the different trends in the GEOS-5 case are artificial.

3.3.2. Sensitivity Analysis

The global-mean trends from AIRS observation and ERA5 reanalysis agree well with each other at this channel, as shown in Figure 4b. Both have a weak positive trend of ~0.1 K/decade with a 95% confidence interval of ~0.1 K/decade. Using the ERA5 monthly profiles, we calculated the trends caused by the change of atmospheric humidity and the change of atmospheric temperature, respectively (the contribution of surface temperature to this channel is very small). Similar to the case of window channels, changes in temperature and humidity contribute oppositely to the trend. Varying humidity alone leads to a negative linear trend of -0.27 ± 0.09 K/decade, and varying air temperature alone leads to a linear trend of 0.33 ± 0.15 K/decade. Their summative effect is then a weak positive trend of 0.07 ± 0.07 K/decade, which is close to the trend derived from the full 6-hourly ERA5 simulation, that is, 0.1 ± 0.1 K/decade.
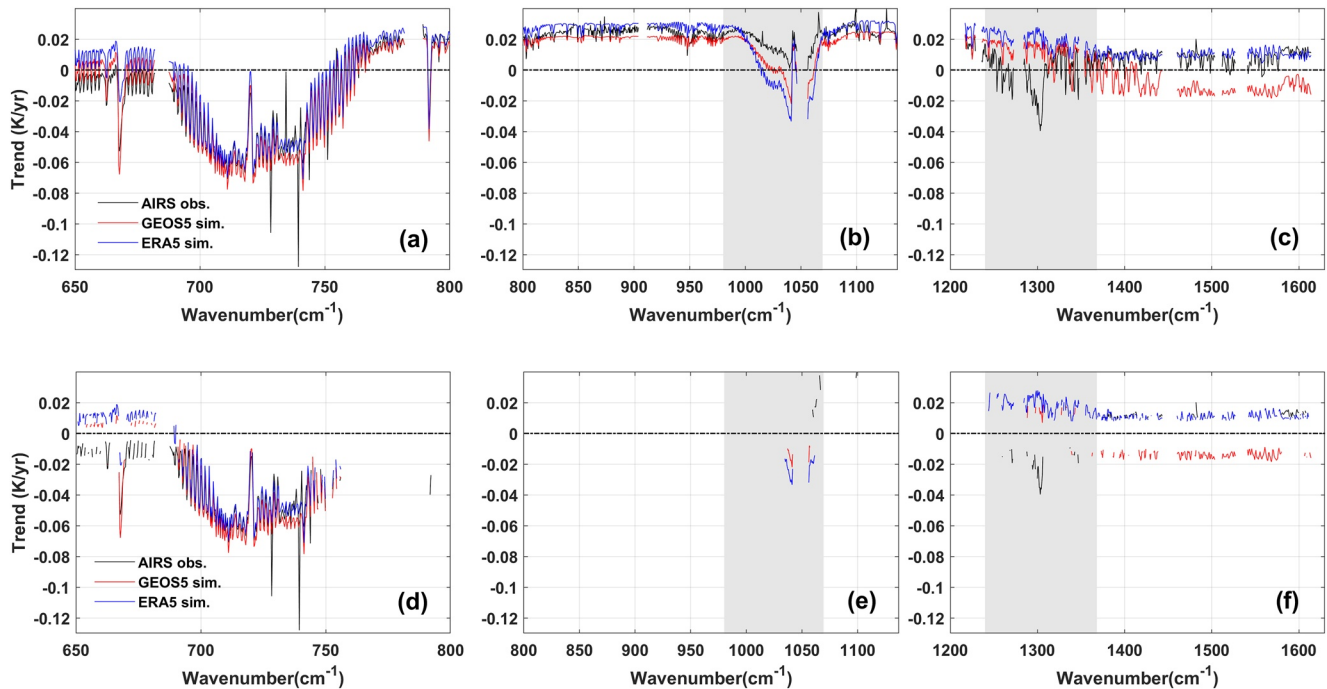
Figure 8. (a–c) the observed and simulated linear trends of all Atmospheric Infrared Sounder mid-IR channels. As in Figure 2, three panels are used for better visualization. (d–f) Same as (a–c), respectively, except only the statistically significant trends (5% significance) are shown. Like in Figure 1, the gray shade columns indicate spectral regions with strong absorptions by trace gases other than H_2O and CO_2 (i.e., ozone for 980–1,070 cm^{-1} and N_2O and CH_4 for 1,240–1,368 cm^{-1}).

4. Trends of All AIRS Mid-IR Channels

The linear trends of all AIRS mid-IR channels for the 2003–2020 period are shown in Figures 8a–8c, while Figures 8d–8f show the statistically significant trends only. Many stratospheric channels in the CO_2 band, that is, the channels between 650 and 690 cm^{-1}, show statistically significant negative trends in the AIRS observation but statistically significant positive trends in the ERA5 and GEOS-5 simulations (Figure 8d). Such opposite trends between observations and reanalyzes reflect issues in the assimilated stratospheric temperatures. AIRS observation and two reanalyzes agree well with each other over the tropospheric channels in the CO_2 band (~690–750 cm^{-1}), all showing statistically significant negative trends. While both reanalyzes largely agree with the AIRS observations in the window region for a generally weak positive trend (Figure 8b), few of them are statistically significant (Figure 8e). Most channels in the H_2O v_2 band are sensitive to the middle and upper stratosphere. For the reasons discussed in Section 3.3.1, GEOS-5 shows negative trends over such channels (Figures 8c and 8f) due to the MHS failure after November 2019. The AIRS observations and ERA5 agree with each other over a majority of channels in the H_2O bands with a positive trend, most of which are statistically significant (Figure 8f). Note that AIRS observations show statistically significant negative trends in the center of the CH_4 band, that is, around 1,306 cm^{-1}, while the trends from GEOS-5 and ERA5 are both positive (Figures 8c and 8f). Since CH_4 variation has not been considered in the simulation, such contrast indicates that the increases of CH_4 concentration from 2003 to 2020 is prominently detectable from the IR hyperspectral observations.

Using the same approach described in Section 3, we further examined the contribution of different variables to the linear trends of ERA5 synthetic radiances. The findings are largely consistent with what has been discussed in Section 3 for the four representative channels. Figure 9a shows that, over the stratospheric channels, the CO_2 variation alone leads to positive trends, and the temperature variation alone leads to a negative trend at a comparable magnitude. As for the tropospheric channels in the CO_2 band, the negative trends caused by the CO_2 variation alone are much larger than the positive trend by the temperature variation, and the summation of two individual trends agrees well with the trend derived from the full simulation. The trends in the window channels are largely decided by the surface temperature changes, while the contributions from air temperature and humidity largely cancel each other (Figure 9b). The weak positive trends in the H_2O bands (Figure 9c) can also be well approxi-
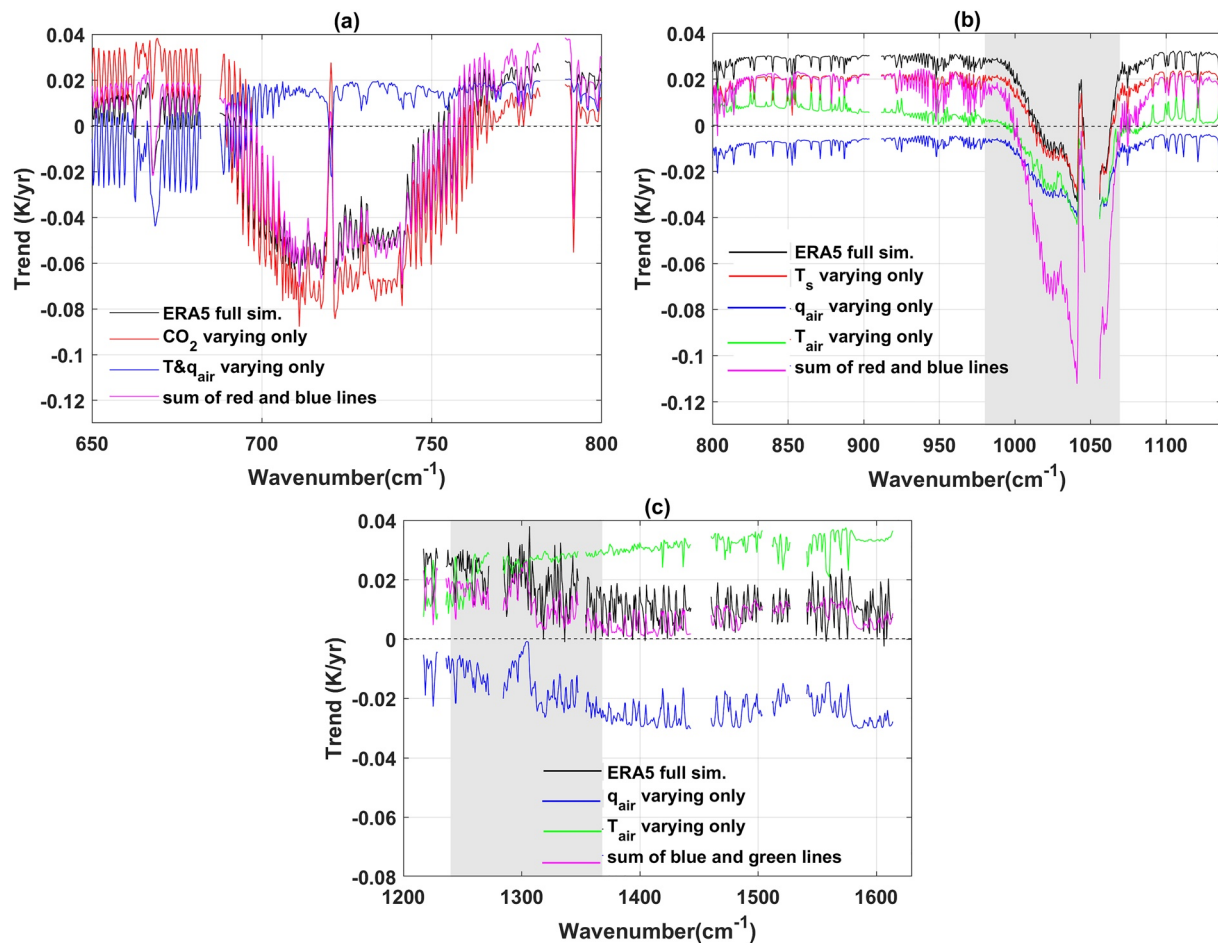
Figure 9. Black lines in (a–c) are the trends derived from synthetic radiances based on ERA5 reanalysis for all Atmospheric Infrared Sounder mid-IR channels. (a) The trend due to varying CO_2 only is shown in red, and due to varying temperature and humidity is shown in blue. The pink line is the summation of the red and blue lines. (b) The trends due to varying surface temperature, atmospheric humidity, and atmospheric temperature are shown in red, light blue, and green, respectively. The pink line is the summation of red, blue, and green lines. (c) The trends due to varying atmospheric humidity alone and atmospheric temperature alone are shown in blue and green, respectively. The pink line is the summation of blue and green lines. The gray shades in (b, c) are spectral regions with significant absorption and emissions from trace gases other than CO_2 and H_2O.

mated by the sum of positive trends due to air temperature change alone and negative trends due to atmospheric humidity change alone.

5. Conclusions and Discussions

Using the collocated observations to identify AIRS clear-sky footprints enabled us to archive a long-term record of nadir-view, clear-sky hyperspectral radiances. The superb instrument performance of AIRS makes such radiance time series an invaluable record for climate studies. This study depicts the trend of global-mean, nadir-view AIRS radiances from 2003 to 2020 and how well such trends can be simulated using two reanalysis data sets, ERA5 and GEOS 5.4.1. ERA5 assimilated AIRS observations, while GEOS 5.4.1 deliberately excluded AIRS and other hyperspectral radiances for its purpose. AIRS observations show negative trends in the majority of CO_2 channels. While the trends derived from simulated radiances from ERA5 and GEOS-5 agree well with those of AIRS over the tropospheric channels in the CO_2 band, the trends from reanalyzes have the opposite sign from those of AIRS over the stratospheric channels in the CO_2 band. Trends in all CO_2 channels can be well approximated by the sum of two individual trends, one due to CO_2 variations alone and the other due to temperature and humidity variations. The trends over the window channels are positive but statistically insignificant; such trends are primarily decided by the surface temperature changes, and the contributions from air temperature and humid-

ity largely offset each other. The AIRS observations have positive trends over its H_2O channels, though not all are statistically significant. ERA5 simulation agrees well with the AIRS observation in terms of the linear trend in the H_2O v_2 band, and such trends can also be approximated by the sum of two trends, one due to air temperature change alone (positive trend) and the other due to humidity change alone (negative trend). The sudden drop of GEOS-5 radiances in the water vapor bands can be attributed to the incorrect assimilation of MHS radiances after the failure of MHS in November 2019. While other trace gases are not the focus of this study, observed and simulated trends at channels with strong CH_4 absorptions do show that the observed trends can only be explained with the CH_4 variation taken into account.

While this study focuses on the global-mean statistics and linear trends, the clear-sky radiances data set can be used to study regional statistics and spatially dependent trends as well. It can also be used in the optimal fingerprinting framework to carry out detection and attribution studies, similar to the stratospheric channel case studies by Pan et al. (2017). Hyperspectral radiance is unique because, in one data set, it reveals spectral details of both radiative forcings of greenhouse gases and several radiative feedbacks, namely Planck feedback, lapse-rate feedback, longwave water vapor feedback, and longwave cloud feedback. More future work can be carried out to exploit such radiance data sets for climate monitoring as well as detection and attribution studies.

Data Availability Statement

The data used for trend analysis in this study, such as time series of global-mean clear-sky BTs from AIRS observations, from synthetic radiances using GEOS-5 and ERA5 data, and differences in clear-sky BT due to AIRS spectral shift, are available at Zenodo via https://doi.org/10.5281/zenodo.7192258. The AIRS L1b radiance data can be obtained via http://airsl1.gesdisc.eosdis.nasa.gov/data/Aqua_AIRS_Level1/AIRIBRAD.005/. The ERA5 data (Hersbach et al., 2018a, 2018b) can be downloaded from https://www.ecmwf.int/en/forecasts/datasets/reanalysis-datasets/era5. Global-mean CO_2 data (Dlugokencky & Tans, 2021), was downloaded from https://gml.noaa.gov/ccgg/trends/gl_data.html. GEOS-5.4.1. data can be requested from Global Modeling and Assimilation Office at NASA Goddard Space Flight Center.

References

Aumann, H. H., Broberg, S., Elliott, D., Gaiser, S., & Gregorich, D. (2006). Three years of AIRS radiometric calibration validation using sea surface temperatures. *Journal of Geophysical Research*, *111*(D16), D16S90. https://doi.org/10.1029/2005JD006822

Aumann, H. H., & Pagano, T. S. (2008). Using AIRS and IASI data to evaluate absolute radiometric accuracy and stability for climate application. In *Atmospheric and environmental remote sensing data processing and utilization IV: Readiness for GEOSS II*. Spie-Int Soc Optical Engineering. https://doi.org/10.1117/12.795225

Chahine, M. T., Pagano, T. S., Aumann, H. H., Atlas, R., Barnet, C., Blaisdell, J., et al. (2006). AIRS: Improving weather forecasting and providing new data on greenhouse gases. *Bulletin of the American Meteorological Society*, *87*(7), 911–926. https://doi.org/10.1175/BAMS-87-7-911

Chen, X. H., Huang, X. L., & Liu, X. (2013). Non-negligible effects of cloud vertical overlapping assumptions on longwave spectral fingerprinting studies. *Journal of Geophysical Research: Atmospheres*, *118*(13), 7309–7320. https://doi.org/10.1002/jgrd.50562

Dlugokencky, E., & Tans, P. (2021). NOAA/GML, Globally averaged marine surface monthly mean data [Dataset]. Global Monitoring Laboratory. https://gml.noaa.gov/ccgg/trends/gl_data.html

ESPC Operations. (2020). Metop-A MHS Channel 2 failure due to noise increase. Retrieved from https://www.ospo.noaa.gov/data/messages/2020/MSG045230402.html

Goody, R., Anderson, J., & North, G. (1998). Testing climate models: An approach. *Bulletin of the American Meteorological Society*, *79*(11), 2541–2549. https://doi.org/10.1175/1520-0477(1998)079<2541:TCMAA>2.0.CO;2

Hanel, R. A., & Conrath, B. J. (1970). Thermal emission spectra of the Earth and atmosphere from the Nimbus 4 Michelson interferometer experiment. *Nature*, *228*(5267), 143–145. https://doi.org/10.1038/228143a0

Haskins, R. D., Goody, R. M., & Chen, L. (1997). A statistical method for testing a general circulation model with spectrally resolved satellite data. *Journal of Geophysical Research*, *102*(D14), 16563–16581. https://doi.org/10.1029/97JD00897

Hersbach, H., Bell, B., Berrisford, P., Biavati, G., Horányi, A., Muñoz Sabater, J., et al. (2018a). ERA5 hourly data on pressure levels from 1979 to present [Dataset]. Chang. https://cds.climate.copernicus.eu

Hersbach, H., Bell, B., Berrisford, P., Biavati, G., Horányi, A., Muñoz Sabater, J., et al. (2018b). ERA5 hourly data on single levels from 1979 to present [Dataset]. Chang. https://cds.climate.copernicus.eu

Hersbach, H., Bell, B., Berrisford, P., Hirahara, S., Horányi, A., Muñoz-Sabater, J., et al. (2020). The ERA5 global reanalysis. *Quarterly Journal of the Royal Meteorological Society*, *146*(730), 1999–2049. https://doi.org/10.1002/qj.3803

Huang, X. L., Chen, X. H., Potter, G. L., Oreopoulos, L., Cole, J. N. S., Lee, D. M., & Loeb, N. G. (2014). A global climatology of outgoing longwave spectral cloud radiative effect and associated effective cloud properties, *Journal of Climate*, *27*, 7475–7492. https://doi.org/10.1175/JCLI-D-13-00663.1

Huang, X. L., Chen, X. H., Zhou, D. K., & Liu, X. (2016). An observationally based global band-by-band surface emissivity dataset for climate and weather simulations. *Journal of the Atmospheric Sciences*, *73*(9), 3541–3555. https://doi.org/10.1175/jas-d-15-0355.1

Huang, X. L., Yang, W. Z., Loeb, N. G., & Ramaswamy, V. (2008). Spectrally resolved fluxes derived from collocated AIRS and CERES measurements and their application in model evaluation: 1. Clear sky over the tropical oceans. *Journal of Geophysical Research*, *113*(D9), D09110. https://doi.org/10.1029/2007JD009219

Huang, X. L., & Yung, Y. L. (2005). Spatial and spectral variability of the outgoing thermal IR spectra from AIRS: A case study of July 2003. *Journal of Geophysical Research*, *110*(D12), D12102. https://doi.org/10.1029/2004JD005530

Iacono, M. J., & Clough, S. A. (1996). Application of infrared interferometer spectrometer clear sky spectral radiance to investigations of climate variability. *Journal of Geophysical Research*, *101*(D23), 29439–29460. https://doi.org/10.1029/96JD02585

Liou, K.-N. (2002). *An introduction to atmospheric radiation*. Elsevier.

Liu, X., Smith, W. L., Zhou, D. K., & Larar, A. (2006). Principal component-based radiative transfer model for hyperspectral sensors: Theoretical concept. *Applied Optics*, *45*(1), 201–209. https://doi.org/10.1364/AO.45.000201

Loeb, N. G., Manalo-Smith, N., Kato, S., Miller, W. F., Gupta, S. K., Minnis, P., & Wielicki, B. A. (2003). Angular distribution models for top-of-atmosphere radiative flux estimation from the clouds and the Earth's radiant energy system instrument on the tropical rainfall measuring mission satellite. Part I: Methodology. *Journal of Applied Meteorology*, *42*(2), 240–265. https://doi.org/10.1175/1520-0450(2003)042<0240:ADMFTO>2.0.CO;2

Manabe, S., & Wetherald, R. T. (1967). Thermal equilibrium of the atmosphere with a given distribution of relative humidity. *Journal of the Atmospheric Sciences*, *24*(3), 241–259. https://doi.org/10.1175/1520-0469(1967)024<0241:TEOTAW>2.0.CO;2

McNally, A. P., & Watts, P. D. (2003). A cloud detection algorithm for high-spectral-resolution infrared sounders. *Quarterly Journal of the Royal Meteorological Society*, *129*(595), 3411–3423. https://doi.org/10.1256/qj.02.208

McNally, A. P., Watts, P. D., Smith, J. A., Engelen, R., Kelly, G. A., Thépaut, J. N., & Matricardi, M. (2006). The assimilation of AIRS radiance data at ECMWF. *Quarterly Journal of the Royal Meteorological Society*, *132*(616), 935–957. https://doi.org/10.1256/qj.04.171

Minnis, P., Sun-Mack, S., Chen, Y., Chang, F.-L., Yost, C. R., Smith, W. L., et al. (2020). CERES MODIS cloud product retrievals for Edition 4, Part I: Algorithm changes. *IEEE Transactions on Geoscience and Remote Sensing*, *59*(4), 2744–2780. https://doi.org/10.1109/TGRS.2020.3008866

Pagano, T. S., Aumann, H. H., Hagan, D. E., & Overoye, K. (2003). Prelaunch and in-flight radiometric calibration of the Atmospheric Infrared Sounder (AIRS). *IEEE Transactions on Geoscience and Remote Sensing*, *41*(2), 265–273. https://doi.org/10.1109/TGRS.2002.808324

Pan, F., Huang, X. L., Guo, H., & Strow, L. L. (2015). Linear trends and closures of 10-year observations of AIRS stratospheric channels. *Journal of Climate*, *28*(22), 8939–8950. https://doi.org/10.1175/JCLI-D-15-0418.1

Pan, F., Huang, X. L., Leroy, S. S., Lin, P., Strow, L. L., Ming, Y., & Ramaswamy, V. (2017). The stratospheric changes inferred from 10 years of AIRS and AMSU-A radiances. *Journal of Climate*, *30*(15), 6005–6016. https://doi.org/10.1175/JCLI-D-17-0037.1

Raghuraman, S. P., Paynter, D., & Ramaswamy, V. (2019). Quantifying the drivers of the clear sky green house effect, 2000–2016. *Journal of Geophysical Research: Atmospheres*, *124*(21), 11354–11371. https://doi.org/10.1029/2019JD031017

Ramaswamy, V., Collins, W. D., Haywood, J. M., Lean, J., Mahowald, N. M., Myhre, G., et al. (2019). Radiative forcing of climate: The historical evolution of the radiative forcing concept, the forcing agents and their quantification, and applications. *Meteorological Monographs*, *59*, 14.1–14.100. https://doi.org/10.1175/AMSMONOGRAPHS-D-19-0001.1

Ramaswamy, V., Schwarzkopf, M. D., Randel, W. J., Santer, B. D., Soden, B. J., & Stenchikov, G. L. (2006). Anthropogenic and natural influences in the evolution of lower stratospheric cooling. *Science*, *311*(5764), 1138–1141. https://doi.org/10.1126/science.1122587

Rienecker, M. M., Suarez, M. J., Gelaro, R., Todling, R., Bacmeister, J., Liu, E., et al. (2011). MERRA: NASA's modern-era retrospective analysis for research and applications. *Journal of Climate*, *24*(14), 3624–3648. https://doi.org/10.1175/JCLI-D-11-00015.1

Rienecker, M. M., Suarez, M. J., Todling, R., Bacmeister, J., Takacs, L., Liu, H.-C., et al. (2008). *The GEOS-5 data assimilation system—Documentation of versions 5.0.1 and 5.1.0, and 5.2.0*. NASA Tech. Rep. Series on Global Modeling and Data Assimilation NASA/TM-2008-104606 (Vol. 27, p. 92). Goddard Space Flight Center. Retrieved from https://gmao.gsfc.nasa.gov/pubs/docs/Rienecker369.pdf

Seemann, S. W., Borbas, E. E., Knuteson, R. O., Stephenson, G. R., & Huang, H.-L. (2008). Development of a global infrared land surface emissivity database for application to clear sky sounding retrievals from multispectral satellite radiance measurements. *Journal of Applied Meteorology and Climatology*, *47*(1), 108–123. https://doi.org/10.1175/2007JAMC1590.1

Strow, L. L., & DeSouza-Machado, S. (2020). Establishment of AIRS climate-level radiometric stability using radiance anomaly retrievals of minor gases and sea surface temperature. *Atmospheric Measurement Techniques*, *13*(9), 4619–4644. https://doi.org/10.5194/amt-13-4619-2020

Strow, L. L., Hannon, S. E., Machado, S. D., Motteler, H. E., & Tobin, D. C. (2006). Validation of the atmospheric infrared sounder radiative transfer algorithm. *Journal of Geophysical Research*, *111*(D9), D09S06. https://doi.org/10.1029/2005JD006146

Weatherhead, E. C., Reinsel, G. C., Tiao, G. C., Meng, X.-L., Choi, D., Cheang, W.-K., et al. (1998). Factors affecting the detection of trends: Statistical considerations and applications to environmental data. *Journal of Geophysical Research*, *103*(D14), 17149–17161. https://doi.org/10.1029/98JD00995

Wu, W., Liu, X., Yang, Q., Zhou, D. K., & Larar, A. M. (2020). Radiometrically consistent climate fingerprinting using CrIS and AIRS hyperspectral observations. *Remote Sensing*, *12*(8), 1291. https://doi.org/10.3390/rs12081291

Zavyalov, V., Esplin, M., Greenman, M., Scott, D., Esplin, B., Graham, B., et al. (2012). CrIS on NPP: Instrument status and first glance on the instrument in-flight performance. In *The 18th international TOVS study conference*. Retrieved from https://cimss.ssec.wisc.edu/itwg/itsc/itsc18/program/files/links/1.07_Zavyalov_po.pdf